Electronically Reconfigurable Binary Phase Liquid Crystal Reflectarray Metasurface at 108 GHz

Xiaomin Meng*, Maziar Nekovee†, Dehao Wu‡ and Richard Rudd§
*†‡Department of Engineering and Informatics, University of Sussex, United Kingdom. †Quantrom Technologies Ltd.
Email: *xm51@sussex.ac.uk, †m.nekovee@sussex.ac.uk, ‡dehao.wu@sussex.ac.uk,
§Plum Consulting, 10 Fitzroy Square, London, United Kingdom
Email: §richard.rudd@plumconsulting.co.uk

***Abstract*—We have proposed a preliminary design and computation results of a 20 by 20 elements reconfigurable liquid crystal (LC) based binary phase reflectarray metasurface for applications in THz wireless communication. Specifically, we performed full-wave simulations and theoretical calculations on the far-field patterns of our proposed device, and we also developed optimisation routines for both the antenna unit cell design as well as far-field pattern synthesis algorithms. The LC used was modelled after Merck's model GT3-23001. At optimal operation frequency of 108 GHz, the phase difference between ON and OFF state is 177 degrees, and the reflection amplitudes of both states are 0.88. We were able to demonstrate 60 degrees of beam steering, which was achieved together with a (single beam) RCS of -5.8 dBm2, when the device dimension is 20mm by 20mm. The operational bandwidth is plus or minus 2 GHz from central frequency of 108 GHz.**

***Index Terms*—Terahertz, metasurface, reconfigurable reflectarray, liquid crystal, wireless communication**

I. Introduction

A. Motivation and Challenges

With the recent announcement by the FCC [1] on the opening of 95 GHz to 3 THz spectrum for 6G related experimental purposes, the field of commercial wireless communication has officially stepped into the THz region. However, many new challenges arise in the field of THz wireless communication, most notably the issues of high diffraction loss (and the consequent need for line-of-sight paths) and high free space path loss. The small wavelength nature of THz electromagnetic (EM) radiation is problematic as the propagation of EM waves is hindered by objects with dimensions similar to the that of the wavelength, which, at the top of newly opened spectrum, is merely 0.1 mm, making most ordinary objects barriers to THz transmission. This brings THz propagation towards the analogy of visible light propagation, where one must establish point to point links without objects along the path. Traditionally, as has been achieved in the lower frequency spectrums, the line of sight issue had been addressed by the development of complex MIMO systems that exploit environmental multi-path nature; in the THz region, however, due to the transmission losses, it will be highly inefficient and thus impractical to develop these reflecting channels.

This bring us to the other critical challenge in THz wireless communication: the high free space path loss. Traditionally, the problem of free space path loss has been dealt with phased array technologies, which would beamform the transmission signal to combat the losses. However, free space path loss is inversely proportional to the square of frequency, which means that going from 1 GHz to 100 GHz would bring about 10,000 times higher path loss, creating extremely challenging standards for modern phased arrays to satisfy. As a matter of fact, a 28GHz 5G phased array transmitter may integrate 1024 antennas to achieve several Gbps data rate over 200m [14], while a 300 GHz 6G transmitter would in theory require 100,000 antennas in order to achieve similar communication range and data rate, due to the high free space path loss associated at THz frequencies (this can be shown by using the relation between antenna gain and element number, together with the Friis transmission equation).

Because of the variety and extremity of THz challenges, we believe that the solution to efficient THz (or millimetre wave) communication lies in breaking down the bigger problem (phased arrays) into smaller ones (antennas and sources) and solving each one individually, as suggested in one paper [13]. In this paper [13], the author presented the idea of coating indoor areas with graphene-based reconfigurable metasurface, which will allow the reflection of THz waves to be directed according to user inputs. In our

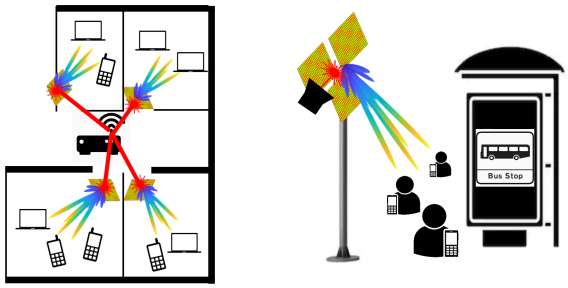

(a) (b)

Fig. 1. A visualisation of the possible application scenarios in connecting beyond-5G users that are in non-line-of-sight (NLOS) locations: a) connecting indoor users that are otherwise in NLOS to the central access point b) "smart-mirror" functioning as short range hotspot, reflecting the signal from integrated source. The laser beam drawing in both figures from source to the device is an indication for our optimism and vision for optical THz sources.

paper we propose a liquid-crystal (LC) based reconfigurable reflectarray metasurface, which can be used as a "smart-relay", helping EM waves to reach NLOS locations through reflection. As shown in FIG-1, the device can be either fed from distant fixed access point, or from an integrated source, whichever option proves to be more power/cost effective. This could be a much more scalable and practical solution to merely boosting phased array performances, as it breaks down the problems associated with phased arrays at THz frequencies (power-inefficiency and high cost) and solves them individually - having a more efficient and powerful THz source (which could be optically-driven, integrated with device) working with a lower power consumption, high efficiency and relatively cheaper "semi-passive" reconfigurable reflectarray metasurface.

B. LC based Reconfigurable Reflectarray Metasurfaces

Reflectarray metasurfaces work in a very similar manner to phased arrays, except instead of generating EM radiation, they reflect incident radiation according to specific designs or inputs. Traditionally, reflectarrays are designed with fixed antennas that are dimensioned to generate a desired reflection pattern; these devices are mostly not reconfigurable, unless mechanically steered. However, recent advancements have introduced reconfigurability in reflectarrays, using either electronic or mechanical methods of adjustments. Due to the small dimensions associated with millimetre waves, mechanical methods, which usually employ MEMS, can be more costly, complex and hence less reliable compared to the electronic counterpart.

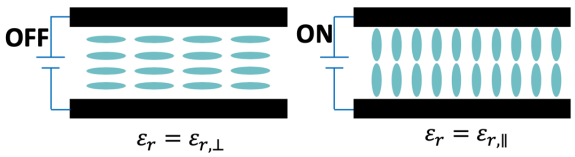

Fig. 2. Molecular alignment of the LC in nematic state. When under applied voltage they exhibit dielectric response on the molecular level, which modifies the parallel/perpendicular component of the permittivity compared to not under electric field, resulting in a phase difference of the antenna radiation

Many recent papers have considered electronically reconfigurable reflectarrays with PIN-diode or LC unit cell designs [2]–[4] in the sub Ka band. In the PIN-diode case, the diode's ON and OFF state corresponds to different dimensions of the antenna elements, hence resulting in drive or lag in the excitation current and causing phase delay/advance. Although effective, PIN-diodes tend to become lossiers in the THz regime due to the parasitic losses [15], making them a relatively inefficient solution of THz reflectarray metasurface. On the other hand, LC does not exhibit such high losses in the THz regime. Reconfigurable LC reflectarrays work on the principle of the anisotropic permittivity nature of nematic state LC, which means that the permittivity of LC can be manipulated through biased voltage, as a result of molecular realignment (FIG-2). Many recent papers have studied LC based reconfigurable reflectarrays, however these have mostly considered using a continuously adjustable source of voltage to control the precise phase difference [10], [11]. This design, although elaborate and precise in beam functionalities, requires much more complexity and power consumption than our proposal, which is a LC reconfigurable reflectarray with binary voltage control, i.e having only two states: ON and OFF.

C. Contribution and Paper Overview

In our study, we propose a LC based reflectarray metasurface that would combine the simplicity in binary phase switching, seen in PIN-diode reconfigurable reflectarrays, with the convenience of LC unit cell design. Our proposed design would directly address the two main challenges in THz wireless communication described above, in terms of NLOS transmission and beamforming. It is important to note that although we have simulated a super lattice of 2cm dimension to save computational costs, the intended device will be larger; either through increasing single device element numbers or through combining multiple 20 by 20 devices to form a collective reflectarray network, as show in FIG-1 b).

In this paper we have developed and implemented a far-field algorithm that will predict the pattern of the electric field in full-wave simulation, given the coding configuration matrix. We present part of our initial codebook configurations for three scenarios: 1) normal incident plane wave, 2) 54° offset plane wave, 3) near-field point source 13 mm away from surface and 20° offset from device centre. For each of these results, we will present 3 subsets of reflection far-field plots: an "all-ON" configuration, an "initial-guess" configuration, and an "optimised" configuration. The "optimised" configuration is achieved through optimising the theoretical beam profile with genetic algorithm, which we are in the preliminary stage of implementation for the purpose of pattern synthesis, as the configuration matrix for even a seemingly simple beam functionality, such as beam-steering, is often non-trivial and only retrievable via numerical methods.

Our proposed metasurface will be capable of different beam manipulations; including, but not limited to, beam-steering, beam-splitting and beamforming. In the following sections we will summarise the theoretical formulations, unit cell optimisation process, theoretical far-field and EM full wave simulation far-fields (demonstrating some of the beam functionalities), followed by some concluding remarks.

II. Problem Setup and Formulations

A. LC Permittivity

Patch antenna dimensions are dependent on the permittivity of the substrate, which in our case is the LC. Numerous sources [6]–[9] have provided this data in the sub THz regime and a few in THz, from which we noticed the independence of ε_r to frequency (19-165 GHz band) of the type GT3-23001. In addition, the operating temperature

of gt3-23001 LC [5] is as wide as -20~100 °C, making it suitable for outdoor applications. Hence we have selected to adapt the GT3-23001 LC, which is commercially available from Merck.

LC type	Frequency (GHz)	$\varepsilon_{r,\perp}$	$\varepsilon_{r,\parallel}$	ref
GT3-23001	19	2.46	3.28	[7]
BL006	35	2.62	3.04	[8]
BL006 Mixture	35	2.3	3.1	[9]
5CB	20	2.2	2.7	[9]
BL037	140-165	2.65	3.25	[6]
GT3-23001	140-165	2.47	3.25	[6]

B. Unit Cell

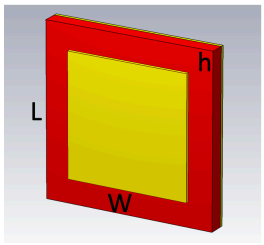

Fig. 3. The schematics of unit cell design. L for periodicity of the system, W for width of the patch antenna and h for height of the LC substrate.

Our device was designed for a unit cell periodicity of 1mm and operational frequency of 108 GHz. The simulated device is composed of 20 by 20 of the unit cell patch antennas. The materials of ground/reflector plate and patch antenna used in simulation are copper. The LC substrate, in ON and OFF state, as aforementioned, are modelled by its permittivity and loss tangent values. In practice, the voltage will be applied through a DC bias connecting the patch and the ground element, creating the necessary electric field to induce permittivity change. The bias mechanism is not included in the full-wave simulation in order to save computational costs without much qualitative effect on the results.

C. Theoretical Far-field

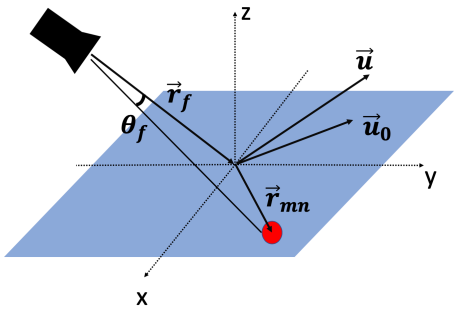

Fig. 4. The geometry definitions used in theoretical formulations.

The far-field pattern can be calculated from the product of pattern function with excitation function:

$$\vec{E}(\hat{u}) = \sum_{m=1}^{M}\sum_{n=1}^{N} \vec{A}_{mn}(\hat{u}) \cdot \vec{I}(\vec{r}_{mn}) \tag{1}$$

here $\hat{u}$ is the unit vector representing the observation direction, expressed as:

$$\vec{u} = \hat{x}\sin\theta\cos\phi + \hat{y}\sin\theta\sin\phi + \hat{z}\cos\theta \tag{2}$$

where $\vec{A}_{mn}$ is the pattern function for mn^{th} unit cell/antenna element, $\vec{I}$ is the excitation function. The unit cell pattern function $\vec{A}_{mn}$ is simplified in scalar form and expressed as:

$$A_{mn}(\theta,\phi) \approx \cos^q(\theta) \cdot e^{ik(\vec{r}_{mn}\cdot\hat{u})} \tag{3}$$

The unit element pattern function accounts for each cell's individual radiation pattern, and it is modelled by cosine raised to the power q function (as patch antennas usually have a rather omni-directional radiation profile), which is also the model used for the feed horn, with appropriate power factor. The exponential term accounts for the propagation from the unit cell.

The excitation function $I(mn)$, which is similar to the array factor, essentially is a sum of the plane waves from each of the unit cell patch antenna centre to an observation point. This accounts for the excitation from the incident plane wave and resulting effects due to the elementary properties of the unit cell antenna, such as amplitude (Γ) and phase ($e^{i\phi_{mn}}$) modification to the reflected wave:

$$I(m,n) \approx \frac{\cos^q\theta_f}{|\vec{r}_{mn}-\vec{r}_f|} \cdot e^{-ik(|\vec{r}_{mn}-\vec{r}_f|)} \cdot |\Gamma_{mn}|e^{i\phi_{mn}} \tag{4}$$

The $\phi_{m,n}$ is the essence of our theory. It is the phase of the mn^{th} reflected wave, it is given by the product of a binary matrix, which accounts for the ON or OFF state of our unit cell, with the phase difference in the reflection given by the change of state. It is the $\phi_{m,n}$ matrix that will be optimised in our GA algorithm to achieve specific beam functionality.

$$\phi_{m,n} = \begin{bmatrix} 1/0 & 1/0 & \dots & 1/0 \\ 1/0 & 1/0 & \dots & 1/0 \\ \vdots & \vdots & \ddots & \vdots \\ 1/0 & 1/0 & \dots & 1/0 \end{bmatrix} \cdot \phi_\Delta \tag{5}$$

The excitation function also includes consideration of the horn-to-unit element transmission distance, which is embedded in the θ_f angles; this is the angle between the illuminating horn and the unit element, as depicted in FIG-4. Finally, combining the above expressions, we can arrive at the electric field profile, or the radiation pattern function, which will be used in the theoretical far-field calculations:

$$E(\theta,\phi) = \sum_{m=1}^{M}\sum_{n=1}^{N} \cos^{q}\theta \frac{\cos^{q}\theta_f}{|\vec{r}_{mn}-\vec{r}_f|} \cdot e^{-ik(|\vec{r}_{mn}-\vec{r}_f|-\vec{r}_{mn}\cdot\hat{u})}\Gamma_{mn} \cdot e^{i\phi_{mn}} \tag{6}$$

III. Numerical Simulations

The primary computational softwares used in this research are CST Studio Suite and Matlab. Studio Suite accounts for the EM simulations carried out in this work, which solves Maxwell's equations with Finite Integral (FI) and Finite Difference Time Domain (FDTD) methods; specifically we have used the Transient and Frequency Domain solvers for our problem. Matlab is is used for the theoretical far-field plots and beam-functionality optimisation.

A. Unit Cell Optimisation

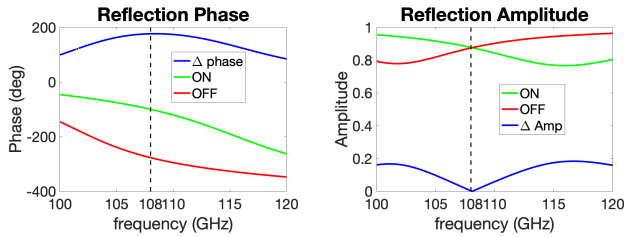

(a) (b)

Fig. 5. a) Ideal operating frequency at 108 GHz, where the reflected amplitude of ON and OFF elements are minimised b)At 108 GHz, the equal reflection frequency for both ON/OFF state, the phase difference is at optimised value of roughly 180°

The unit cell antenna element design is a task shared by computations across both software platforms. We first adopt a rough design of antenna element for a desired frequency range and LC type, in our case, 123 GHz and Merck's GT3-23001 LC. Next, S-parameter calculations are carried out with periodic boundary conditions and the Floquet solver, on both the ON and OFF states of the LC (which is simulated with the difference in permittivities and loss tangents). From these simulations we can retrieve two important properties: 1) the phase difference and 2) the amplitude difference, between the reflected EM wave on the unit cell when LC is in the ON state versus the OFF state.

Next, we exercise the parameter sweep function, which allows us to optimise the structure's parameters for performance. In parameter sweep, we specifically aim to optimise both the S11 amplitude and S11 phase, where S11 value is maximised and a S11 phase difference of π is aimed for between the ON and OFF state of the LC. This optimisation is achieved through Matlab, after exporting the S11 results from Studio Suite. It is important to note that the S-parameter optimisation is different than that in traditional antenna design, which involves the excitation sourcing through feedline and scattering parameters measured on a

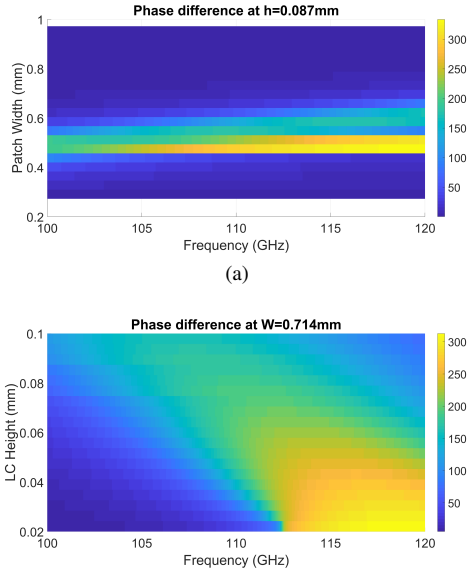

(a) (b)

Fig. 6. a) Optimisation visualisation for variation in parameters h (LC height) and the effect on the phase difference between ON and OFF state b) similar plot for variation in parameter W (patch width). The "low-resolution" effect is due to the large simulation step-size.

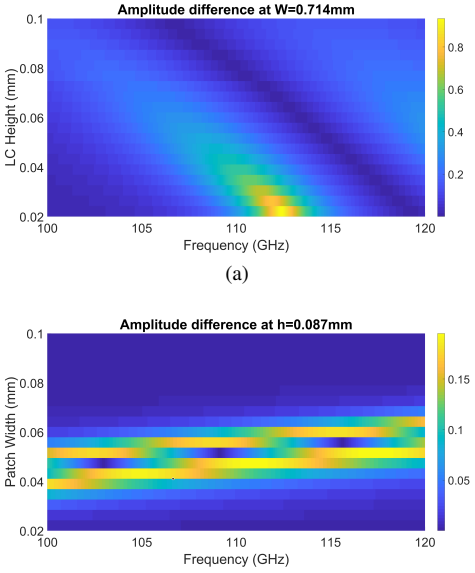

(a) (b)

Fig. 7. a) and b) corresponding parameter sweep and effect on reflection amplitude difference. Note the amplitude difference is then conditionally filtered to user defined lower bound (for example, 0.8).

cross-section through the feedline; in our case, the patch is parasitic and does not contain a feedline for excitation, and more notably, the plane at which S-parameters are calculated is parallel to our antenna, rather than perpendicular to it. This is the due to the fact the radiated EM wave from unit cell antenna is actually the reflected EM wave. Therefore, in our optimisation, we actually optimise the structure for maximum S-11 reflection, subject to the constraint of 1) 180° phase difference, 2) minimum reflection amplitude

difference.

The results have shown that our device achieves phase difference of 177° and reflection amplitude of 0.88 at the designed frequency of 108.1 GHz. The bandwidth is usually defined by 3 dB far field strength drop, however in our case, we observe that although the device is able to maintain less than 3 dB drop beyond 108 ± 2 GHz, the far field start to generate significant sidelobe in undesired locations, which we consider unacceptable behaviour. Thus we have kept the bandwidth of ± 2 GHz, which is far below 3 dB drop, however ensuring no significant sidelobe in unwanted directions.

B. Full-device

We have simulated the 20 by 20 metasurface reflection radiation pattern, given various combinations of ON and OFF states of the LC unit cell. Here we present three sets of far-field plot results: 1) source is normal incident far-field plane wave on canonical combinations, 2) source is 54° offset far-field plane wave, 3) source is near-field feed horn located at offset position of $L \cdot [-4.5; 0, 13]$ from the centre. On the second and third set of the plots, we have also shown our preliminary optimisation results.

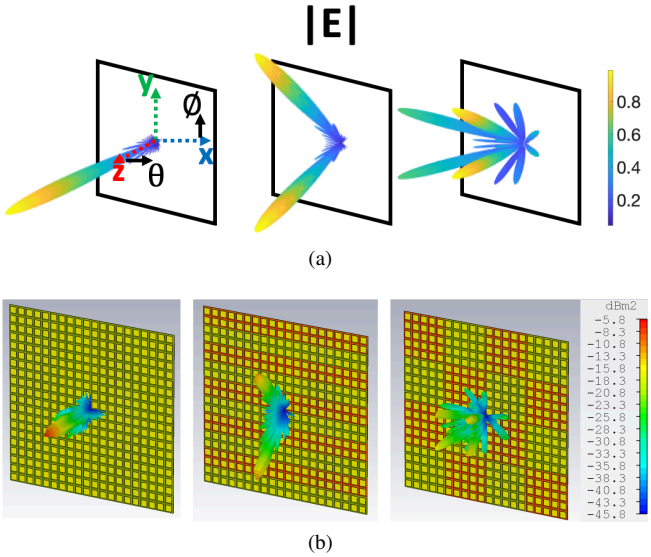

Fig. 8. The red unit cell represents OFF while green for ON state. For a linearly polarised (in x direction) normal incident plane wave, a) theoretical far field pattern calculations of reflected wave for configurations of all ON, parallel ON's and OFF's and checkerboard ON's and OFF's, normalised to their maximums b) full-wave simulation of the corresponding configurations. Note the device dimension is 20mm by 20mm, so at single beam peak Radar Cross Section (RCS) of -5.8 dBm2, it is equivalent of linear RCS of $260mm^2$.

The far-field patterns in FIG-8 are produced from normally-incident linearly-polarised (along x) plane waves, and are consistent with the results of some of the lower frequency PIN-diode based binary phase reflectarray papers [2], [3], given the same configuration. The normal incident plane wave is the least likely scenario in terms of application, this is because if a feed is used, then it will be positioned above our device, which then causes inevitable blockage/blind-spot from the horn; even if impinging wave is from far-field, the normal incident wave proves ineffective in beamsteering abilities, due to the lack of a continuous phase shift, which is naturally present in offset feed. However, we performed these simulations to confirm that our theoretical model and full wave simulation are in accordance, before moving onto the realistic scenarios and applying optimisation algorithms for pattern synthesis. Note that RCS is used for the far field here, as the device is scattering an incoming plane wave, making dBi rather irrelevant due to the passive nature of the device.

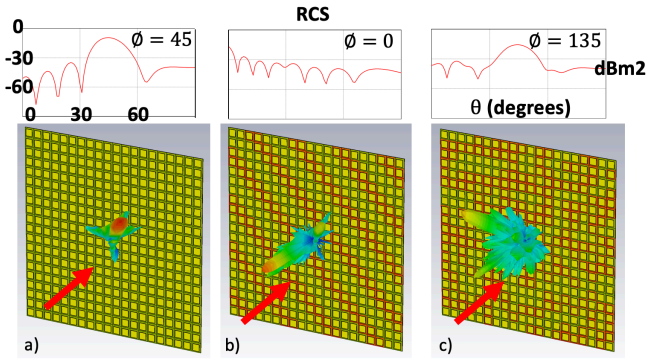

Fig. 9. The full wave simulation of $\theta = 54^\circ$ offset far-field source plane wave (red arrow indicating direction of incidence) on a) all ON configuration b) initial guess of reverse beamsteering configuration c) GA optimised beamsteering at $\theta = 45^\circ$ and $\phi = 135^\circ$. The overhead 2D plot is chosen at specific ϕ angles to demonstrate the mainlobe direction in θ.

In FIG-9 we have simulated an offset far-field source located 26 meters away and at 54° angle to device plane. As expected, when the device is in the "all-ON" configuration as shown in FIG-9 a), it behaves as a reflector, resulting in a far-field pattern that is identical to incident beam, but opposite in direction. In FIG-9 b) we have presented an anomalous reflection configuration, which essentially steers the beam towards the normal direction to device plane. FIG-9 c) is the GA optimisation according to our desired beamsteering direction, which in this case is set to $\theta = 45^\circ$ and $\phi = 135^\circ$.

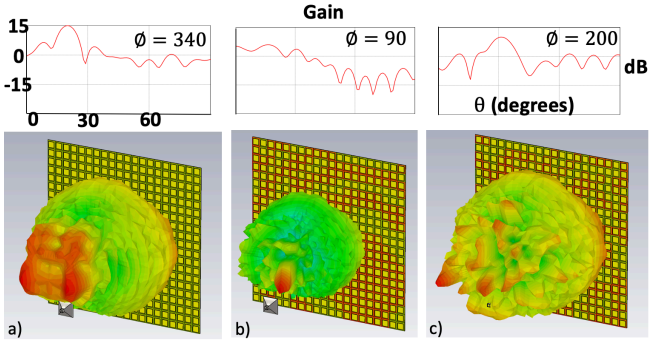

Fig. 10. The full wave simulation of $\theta = 20^\circ$ offset near-field point source feed on a) all ON configuration b) initial guess for beamsteering configuration c) preliminary GA optimised multibeam with mainlobe at $\theta = 30^\circ$ and $\phi = 200^\circ$.

In FIG-10 we have simulated an offset near-field point-like source located at $L \cdot [-4.5; 0, 13]$ with respect to the centre, as shown in figure. Note that because of the use of a realistic far field source with specific power parameters (rather than the fictitious plane wave in previous figures), the units for far-field here are in dBi. It is important to point out that the gain in dB for results in FIG-10 can be even higher, due to the fact that our feed horn is not optimised, and as a result portion of impinging EM radiation from the feed horn is missing the device's surface. The multibeam intended in FIG-10 c) is a three beam profile, however, other than the three intended beams, there are many high level sidelobe beams. We are in the process of improving the performance of GA through (such as adjustments of cost function), in order to not only achieve beam-directivity, but also reduction in sidelobe levels.

We have, and are currently still updating, a codebook of different combinations of the ON/OFF, primarily for the second and third scenario (offset far-field, and offset near-field feed horn). This could be advantageous in a few ways: firstly, we can adopt some of the configurations from our codebook as starting population for GA pattern synthesis; secondly, the codebook can eventually be stored either onboard or delivered to the device from source.

IV. Conclusions

We have proposed and optimised a LC based binary phase reconfigurable reflectarray metasurface for 108 GHz operation. At optimal operation frequency of 108 GHz, the phase difference between ON and OFF state is 177 degrees, and the reflection amplitudes of both states are 0.88. We were able to demonstrate 60 degrees of beam steering, which was achieved together with a single beam RCS of -5.8 dBm2. The device dimension is 20mm by 20mm. The operational bandwidth is plus or minus 2 GHz from central frequency of 108 GHz.

With the aid of software simulation, we have performed both theoretical calculation and full-wave simulations of the far-field. With GA, we were able to attain preliminary results for beam functionalities, such as beam steering and multi-beam splitting, though further work is needed on acquiring more accurate and higher quality beam-functionalities, also the efficiency GA algorithm needs to be improved for faster pattern synthesis.

In terms of the practicality and limitations of the device, one of the main issues would be the small aperture size, which is on the decimetre order, even when working with multiple surfaces. Thus, beam-formed source waves with narrow beamwidth will be needed for an efficient performance. Powerful and yet affordable THz sources is another challenge for potential commercialisation of this type of device. Finally, the biasing circuit controls need to be designed and investigated for most practical and efficient solution to controlling the 400 individual elements.

For future work, our first priority is at reinforcing the pattern synthesis algorithm for better performances, such as readjusting the GA operations and cost functions, and introducing 2D discrete inverse Fourier transform for faster synthesis progress. Next, we will develop an optimised feed horn, with which we will also look into the simulation of multiple 20 by 20 devices working cooperatively. At a later stage, we aim to develop a prototype of the metasurface for testing. Additionally, we also intend to adopt better unit cell performances, such as wider resonance bandwidth through introduction of more complex unit cell patch antenna designs, with fractal structure, or even multi-resonance antenna patches.

Acknowledgment

We would like to thank Dr. Junaid Syed from Rosenberger for the helpful discussions on this work.

References

[1] Jeremy Horwitz: "FCC opens 95GHz to 3THz spectrum for 6G, 7G, or whatever is next", *https://venturebeat.com/2019/03/15/fcc-opens-95ghz-to-3thz-spectrum-for-6g-7g-or-whatever-is-next/*, 03/15/2019

[2] Xiang Wan, Meiqing Qi, Tianyi Chen, Tiejun Cui: "Field-programmable Beam Reconfiguring based on Digitally-Controlled Coding Metasurface", *Scientific Reports*, 2016, **6**

[3] HuanHuan Yang, Xiangyu Cao, Fan Yang, Jun Gao, Shenheng Xu, Maokun Li, Xibi Chen, Yi Zhao, Yuejun Zheng, Sijia Li: "A Programmable Metasurface with Dynamic Polarization, Scattering and Focusing Control", *Scientific Reports*, 2016, **6**

[4] Tiejun Cui, Meiqing Qi, Xiang Wan, Jie Zhao, Qiang Cheng: "Coding Metamaterials, Digital Metamaterials and Programmable Metamaterials", *Light: Science and Applications*, 2014, **3**

[5] PouriaYaghmaee: "Reconfigurable Tunable Microwave Devices Using Liquid Crystal", *PhD Thesis*, 2014

[6] R. Dickie, P. Baine, R. Cahill, E. Doumanis, G. Goussetis, S. Christie, N. Mitchell, V. Fusco, D. Linton, J. Encinar, R. Dudley, D. Hindley, M. Naftaly, M. Arrebola and G. Toso: "Electrical Characterisation of Liquid Crystals at Millimetre Wavelengths Using Frequency Selective Surfaces ", *Electronic Letters*, 2012, **48**, no. 11

[7] P. Yagmaee, W. Withayachumnajul, A. K. Horestani, A. Ebrahimi: "Tunable Electric-LC Resonators Using Liquid Crystal", *IEEE*, 2013, **978**, pp. 382–383

[8] A. Moessinger, R. Marin, J. Freese, S. Mueller, A. Manabe, R. Jakoby: "Investigation on 77GHz Tunable Reflectarray Unit Cells with Liquid Crystal", *Pro. EuCAP*, 2006

[9] A. Karim, H. Yadav, S. Ahmad: "Design and Simulation of LC Based Patch Antenna at 20 GHz Frequency", *AIP Conference Proceedings*, 2014, **1620**, pp. 15-21

[10] Saygin Bildik, Sabine Dieter, Carsten Fritzsch, Michael Frei, Christoph Fischer, Wolfgang Menzel, Rolf Jakoby: "Reconfigurable Liquid Crystal Reflectarray with Extended Tunable Phase Range", *Proceedings of the 41st European Microwave Conference*, 2011, **978**, pp.1292-1294

[11] Perez-Palomino, G., Barba, M., Encinar, J., Cahill, R., Dickie, R., and Baine: "Liquid Crystal Based Beam Scanning Reflectarrays and Their Potential in SATCOM Antennas", *Proceedings of EuCAP 2017*, 2017

[12] M. Y. Ismail, M. Inam: "Liquid Crystal Based Reflectarray Antenna Design", *International Scholarly and Scientific Research and Innovation*, 2016, **10**, 2017

[13] Ian F. Akyildiz, Chong Han, Shuai Nie: "Combating the Distance Problem in the Millimeter Wave and Terahertz Frequency Bands", *IEEE Communications Magazine*, 2018

[14] David Chambers: "Verizon/Samsung 5G Fixed Wireless Trials proving a success", *https://www.thinksmallcell.com/5G/verizon-samsung-5g-fixed-wireless-trials-proving-a-success.html*, 10/05/2018

[15] Afaque Karim, Harsh Yadav, Shakeb Ahmad: "Design and Simulation of LC Based Patch Antenna @ 20 GHz Frequency", *AIP Conference Proceedings*, **1620**, 2014